A Model free Stress Approximation

Project-II (CE47006) report submitted to

Indian Institute of Technology Kharagpur

in partial fulfilment for the award of the degree of

Bachelor of Technology

in

Civil Engineering

by

Sadique Amin

(21CE31011)

Under the supervision of

Professor Biswanath Banerjee

Department of Civil Engineering

Indian Institute of Technology Kharagpur

Spring Semester, 2024-25

June 2, 2025

DECLARATION

I certify that

(a) The work contained in this report has been done by me under the guidance of my supervisor.

(b) The work has not been submitted to any other Institute for any degree or diploma.

(c) I have conformed to the norms and guidelines given in the Ethical Code of Conduct of the Institute.

(d) Whenever I have used materials (data, theoretical analysis, figures, and text) from other sources, I have given due credit to them by citing them in the text of the thesis and giving their details in the references. Further, I have taken permission from the copyright owners of the sources, whenever necessary.

Date: June 1, 2025 (Sadique Amin)

Place: Kharagpur (21CE31011)

DEPARTMENT OF CIVIL ENGINEERING

INDIAN INSTITUTE OF TECHNOLOGY KHARAGPUR

KHARAGPUR - 721302, INDIA

CERTIFICATE

This is to certify that the project report entitled "**A Model free Stress Approximation**" submitted by **Sadique Amin** (Roll No. 21CE31011) to Indian Institute of Technology Kharagpur towards partial fulfilment of requirements for the award of degree of Bachelor of Technology in Civil Engineering is a record of bona fide work carried out by him under my supervision and guidance during Spring Semester, 2024-25.

Date: June 1, 2025
Place: Kharagpur

Professor Biswanath Banerjee
Department of Civil Engineering
Indian Institute of Technology Kharagpur
Kharagpur - 721302, India

Abstract

Name of the student: **Sadique Amin** Roll No: **21CE31011**

Degree for which submitted: **Bachelor of Technology**

Department: **Department of Civil Engineering**

Thesis title: **A Model free Stress Approximation**

Thesis supervisor: **Professor Biswanath Banerjee**

Month and year of thesis submission: **June 2, 2025**

Acknowledgements

I would like to express my heartfelt gratitude to my supervisor, Prof. Biswanath Banerjee, for his invaluable guidance and unwavering support throughout my project work. His insightful direction has been instrumental in shaping my research, providing clarity and purpose to my efforts. Engaging in regular discussions with him proved to be particularly beneficial, as they allowed me to navigate through challenges and uncertainties that arose during the course of my work. His expertise and encouragement not only enhanced my understanding of the subject but also motivated me to strive for excellence. I am truly grateful for his mentorship, which has greatly enriched my academic experience.

Contents

Symbols

$\boldsymbol{\sigma}$, T	Second Piola-Kirchhoff stress tensor
$\boldsymbol{\varepsilon}$, E	Green-Lagrange strain tensor
$\mathbb{C}$	Fourth-order elasticity tensor
$\mathbb{S}$	Constitutive Matrix
$\mathbf{S}$	Stress vector in Voigt notation
$\mathbf{M}$	Fabric tensor (second-order symmetric tensor)
$\mathbf{I}$	Identity matrix
$\mathbf{F}$	Deformation gradient tensor
λ	stretch ratio
λ_0	Reference stretch ratio
λ_0'	Derivative of the reference stretch ratio with respect to strain
μ_0	Initial shear modulus
k	Bulk modulus
$\mathbf{E}_{\text{Mat}}$	Strain vector in Voigt notation
ϕ	Strain energy density function

Chapter 1

Introduction and Literature Review

Overview

The overarching goal of this study is to estimate the elastic behavior of nonlinear materials by leveraging their microstructural characteristics, specifically through the use of the *fabric tensor*—a second-rank tensor that captures the internal directional structure and anisotropy of the material. The fabric tensor, which can be estimated from the deformation gradient obtained through experiments or simulations, provides a compact and physically meaningful way to describe the material's internal architecture. By applying the theoretical framework of fabric tensors, we reduce the number of independent parameters needed to characterize the material's non-linear elastic response to just four: λ_o, λ_o', μ_o, and k. These parameters serve as effective descriptors of the material's constitutive behavior, and their values are determined by minimizing a residual function. This approach enables a computationally efficient and physically grounded method for estimating material properties in the context of anisotropic and non-linear elasticity.

1.1 Understanding the Fabric Tensor and Elasticity Tensor Formulation

1.1.1 Microstructural Influence on Elastic Properties

The behavior of materials at the microscopic level often governs their macroscopic mechanical response. In particular, the mechanical properties of porous or composite materials are influenced not only by their bulk composition but also by the microstructural arrangement of their constituent phases. To quantitatively capture this arrangement, researchers have introduced the concept of the *fabric tensor*. This tensorial descriptor plays a vital role in correlating microstructure with material properties, especially in the study of elasticity.

1.1.2 Fabric Tensor and Volume Fraction

A *fabric tensor*, denoted $\mathbf{M}$ with components M_{ij}, is a symmetric second-rank tensor that characterizes the distribution and orientation of microstructural features in a porous material. It serves as the second principal measure of microstructure after the porosity or solid volume fraction, denoted v. For elastic porous materials, the fabric tensor provides directional information about the internal structure that influences elastic behavior.

1.1.3 Cowin's Representation of Elasticity Tensors

The pioneering work of S. C. Cowin introduced a formal relationship between the fourth-rank elasticity tensor C_{ijkl} and the fabric tensor M_{ij}, assuming isotropic constitutive functions. This representation is given by:

$$\begin{aligned} C_{ijkm} = {} & a_1\delta_{ij}\delta_{km} + a_2(M_{ij}\delta_{km} + \delta_{ij}M_{km}) + a_3(\delta_{ik}M_{kq}M_{qm} + \delta_{km}M_{iq}M_{qj}) \\ & + b_1M_{ij}M_{km} + b_2(M_{ik}M_{kq} + M_{km} + M_{is}M_{sj}M_{km}) + b_3M_{is}M_{sj}M_{kq}M_{qm} \\ & + c_1(\delta_{ki}\delta_{mj} + \delta_{mi}\delta_{kj}) + c_2(\delta_{ik}M_{mj} + \delta_{kj}M_{mi} + \delta_{im}M_{kj} + \delta_{mj}M_{ki}) \\ & + c_3(M_{ir}M_{rk}\delta_{mj} + M_{kr}M_{rj}\delta_{mi} + M_{ir}M_{rm}\delta_{kj} + M_{mr}M_{rj}\delta_{ik}), \end{aligned}$$

where a_i, b_i, and c_i are scalar functions of the solid volume fraction v. This formulation allows for a compact, symmetry-informed model of the elasticity tensor driven by microstructure.

1.1.4 Orthotropic Elasticity and Microstructural Parameters

The representation (4) of the fourth-rank elasticity tensor, though useful, is limited in its ability to capture the full range of elastic material symmetries. In particular, it cannot represent triclinic materials, which exhibit no symmetry, or monoclinic materials, which have only a single plane of reflective symmetry. The minimal symmetry that can be represented by this formulation is orthotropy. This becomes evident when the representation is expanded in indicial notation under the coordinate system that diagonalizes the fabric tensor. In this basis, the off-diagonal components A_{12}, A_{13}, and A_{23} vanish, and A_{11}, A_{22}, and A_{33} become the eigenvalues of the fabric tensor. The resulting expansion of the elasticity tensor yields the following nine non-zero components, which are valid only when the fabric tensor is diagonal:

$$
\begin{aligned}
C_{1111} &= a_1 + 2c_1 + 2(a_2 + 2c_2)A_{11} + (2a_3 + b_1 + 4c_3)A_{11}^2 + 2b_2A_{11}^3 + b_3A_{11}^4,\\
C_{2222} &= a_1 + 2c_1 + 2(a_2 + 2c_2)A_{22} + (2a_3 + b_1 + 4c_3)A_{22}^2 + 2b_2A_{22}^3 + b_3A_{22}^4,\\
C_{3333} &= a_1 + 2c_1 + 2(a_2 + 2c_2)A_{33} + (2a_3 + b_1 + 4c_3)A_{33}^2 + 2b_2A_{33}^3 + b_3A_{33}^4,\\
C_{1122} &= a_1 + a_2(A_{11} + A_{22}) + a_3(A_{22}^2 + A_{11}^2) + b_1A_{11}A_{22} + b_2(A_{11}A_{22}^2 + A_{11}^2A_{22}) + b_3A_{11}^2A_{22}^2,\\
C_{1133} &= a_1 + a_2(A_{11} + A_{33}) + a_3(A_{33}^2 + A_{11}^2) + b_1A_{11}A_{33} + b_2(A_{11}A_{33}^2 + A_{11}^2A_{33}) + b_3A_{11}^2A_{33}^2,\\
C_{2233} &= a_1 + a_2(A_{22} + A_{33}) + a_3(A_{22}^2 + A_{33}^2) + b_1A_{22}A_{33} + b_2(A_{22}A_{33}^2 + A_{33}A_{22}^2) + b_3A_{22}^2A_{33}^2,\\
C_{1212} &= c_1 + c_2(A_{11} + A_{22}) + c_3(A_{11}^2 + A_{22}^2),\\
C_{1313} &= c_1 + c_2(A_{11} + A_{33}) + c_3(A_{11}^2 + A_{33}^2),\\
C_{2323} &= c_1 + c_2(A_{22} + A_{33}) + c_3(A_{22}^2 + A_{33}^2),
\end{aligned}
$$

In a previous approach, we attempted to derive constraints on each of the scalar coefficients a_1, a_2, a_3, b_1, b_2, b_3, c_1, c_2, and c_3 individually. However, the complexity

of the resulting equations made this method analytically and computationally challenging. In this work, we adopt an alternative model proposed by Curnier, which expresses the elasticity tensor in terms of just two components: the fabric tensor and four intrinsic material parameters—λ_o, λ'_o, μ_o, and k. This significantly simplifies the formulation by reducing the number of independent parameters from nine to four, while still capturing the essential anisotropic behavior through the fabric tensor.

1.2 Microstructure-Informed Elasticity Model (Alternative approach)

1.2.1 Fourier Decomposition of Microstructure

The microstructure is characterized by a positive, radially symmetric scalar property with an orientation distribution function $f(\boldsymbol{N})$, where $\boldsymbol{N} = \boldsymbol{n} \otimes \boldsymbol{n}$ and $\boldsymbol{n}$ is a unit vector. The function $f(\boldsymbol{N})$ is expanded in a Fourier series using spherical harmonics:

$$f(\boldsymbol{N}) = g \cdot \mathbf{1} + \boldsymbol{G} : \boldsymbol{F}(\boldsymbol{N}) + \mathbb{G} :: \mathbb{F}(\boldsymbol{N}) + \cdots , \tag{1.1}$$

where g, $\boldsymbol{G}$, and $\mathbb{G}$ are scalar, second-rank, and fourth-rank fabric tensors, respectively, and $\boldsymbol{F}(\boldsymbol{N}) = \boldsymbol{N} - \frac{1}{3}\boldsymbol{I}$. For simplicity, the approximation is truncated:

$$\hat{f}(\boldsymbol{N}) = g \cdot \mathbf{1} + \boldsymbol{G} : \boldsymbol{F}(\boldsymbol{N}), \tag{1.2}$$

with $\boldsymbol{G}$ symmetric and traceless, ensuring orthotropic symmetry. Positivity requires:

$$g > -\min_i\{g_i\}, \tag{1.3}$$

where g_i are the eigenvalues of $\boldsymbol{G}$.

1.2.2 Elastic Free Energy

Assuming the material's mechanical anisotropy matches the microstructure, the elastic free energy $\psi(\boldsymbol{E}, g, \boldsymbol{G})$ is an isotropic function of the strain tensor $\boldsymbol{E}$, g, and $\boldsymbol{G}$. Using representation theorems, the quadratic free energy for linear elasticity is:

$$\begin{aligned}\psi(\boldsymbol{E}, g, \boldsymbol{G}) = &\frac{c_1}{2}\operatorname{Tr}^2(\boldsymbol{E}) + \frac{c_2}{2}\operatorname{Tr}(\boldsymbol{E}^2) + \frac{c_3}{2}\operatorname{Tr}^2(\boldsymbol{E}\boldsymbol{G}) + c_4\operatorname{Tr}(\boldsymbol{E}^2\boldsymbol{G}) \\ &+ \frac{c_5}{2}\operatorname{Tr}^2(\boldsymbol{E}\boldsymbol{G}^2) + \frac{c_6}{2}\operatorname{Tr}((\boldsymbol{E}\boldsymbol{G})^2) + c_7\operatorname{Tr}(\boldsymbol{E})\operatorname{Tr}(\boldsymbol{E}\boldsymbol{G}) \\ &+ c_8\operatorname{Tr}(\boldsymbol{E}\boldsymbol{G})\operatorname{Tr}(\boldsymbol{E}\boldsymbol{G}^2) + c_9\operatorname{Tr}(\boldsymbol{E})\operatorname{Tr}(\boldsymbol{E}\boldsymbol{G}^2),\end{aligned} \tag{1.4}$$

where c_i depend on g and invariants of $\boldsymbol{G}$.

1.2.3 Elasticity Tensor and Homogeneity Assumption

The elasticity tensor is obtained as:

$$\begin{aligned}\mathbb{S} = \frac{\partial^2\psi}{\partial\boldsymbol{E}^2} = &c_1\,\boldsymbol{I}\otimes\boldsymbol{I} + c_2\,\boldsymbol{I}\underline{\otimes}\boldsymbol{I} + c_3\,\boldsymbol{G}\otimes\boldsymbol{G} \\ &+ c_4\,(\boldsymbol{G}\underline{\otimes}\boldsymbol{I} + \boldsymbol{I}\underline{\otimes}\boldsymbol{G}) + c_5\,\boldsymbol{G}^2\otimes\boldsymbol{G}^2 + c_6\,\boldsymbol{G}\underline{\otimes}\boldsymbol{G} \\ &+ c_7\,(\boldsymbol{I}\otimes\boldsymbol{G} + \boldsymbol{G}\otimes\boldsymbol{I}) + c_8\,(\boldsymbol{G}\otimes\boldsymbol{G}^2 + \boldsymbol{G}^2\otimes\boldsymbol{G}) \\ &+ c_9\,(\boldsymbol{I}\otimes\boldsymbol{G}^2 + \boldsymbol{G}^2\otimes\boldsymbol{I}).\end{aligned} \tag{1.5}$$

Using the spectral decomposition $\boldsymbol{G} = \sum_i g_i\boldsymbol{G}_i$, where $\boldsymbol{G}_i = \boldsymbol{g}_i\otimes\boldsymbol{g}_i$, the tensor assumes an orthotropic form:

$$\mathbb{S} = \sum_i \lambda_{ii}\boldsymbol{G}_i\otimes\boldsymbol{G}_i + \sum_{i<j}\lambda^*_{ij}(\boldsymbol{G}_i\otimes\boldsymbol{G}_j + \boldsymbol{G}_j\otimes\boldsymbol{G}_i) + 2\sum_{i<j}\mu_{ij}(\boldsymbol{G}_i\underline{\otimes}\boldsymbol{G}_j + \boldsymbol{G}_j\underline{\otimes}\boldsymbol{G}_i), \tag{1.6}$$

with coefficients:

$$\begin{aligned}\lambda_{ii} &= c_1 + c_2 + c_3 g_i^2 + 2c_4 g_i + c_5 g_i^4 + c_6 g_i^2 + 2c_7 g_i + c_8 g_i^3 + 2c_9 g_i^2, \\ \lambda^*_{ij} &= c_1 + c_3 g_i g_j + c_5 g_i^2 g_j^2 + c_7(g_i + g_j) + c_8(g_i g_j^2 + g_j g_i^2) + c_9(g_i^2 + g_j^2), \\ \mu_{ij} &= \frac{1}{2}c_2 + \frac{1}{2}c_4(g_i + g_j) + \frac{1}{2}c_6 g_i g_j.\end{aligned} \tag{1.7}$$

To simplify the model, Zysset and Curnier (1995) assume a homogeneity property:

$$\mathbb{S}(\lambda g, \lambda \boldsymbol{G}) = \lambda^k \mathbb{S}(g, \boldsymbol{G}), \quad \forall \lambda > 0, \tag{1.8}$$

ensuring scale invariance of the elasticity tensor. Replacing the identity tensor in the classical isotropic model with a homogeneous anisotropic form $(g\boldsymbol{I} + \boldsymbol{G})^k$, they arrive at:

$$\mathbb{S}(g, \boldsymbol{G}) = \lambda_c (g\boldsymbol{I} + \boldsymbol{G})^k \otimes (g\boldsymbol{I} + \boldsymbol{G})^k + 2\mu_c (g\boldsymbol{I} + \boldsymbol{G})^k \underline{\otimes} (g\boldsymbol{I} + \boldsymbol{G})^k. \tag{1.9}$$

In the principal basis of $\boldsymbol{G}$, this yields:

$$\begin{aligned} \mathbb{S}(g, \boldsymbol{G}) = & \sum_i (\lambda_c + 2\mu_c)\, m_i^{2k}\, \boldsymbol{G}_i \otimes \boldsymbol{G}_i \\ & + \sum_{i<j} \lambda_c\, m_i^k m_j^k\, (\boldsymbol{G}_i \otimes \boldsymbol{G}_j + \boldsymbol{G}_j \otimes \boldsymbol{G}_i) \\ & + 2 \sum_{i<j} \mu_c\, m_i^k m_j^k\, (\boldsymbol{G}_i \underline{\otimes} \boldsymbol{G}_j + \boldsymbol{G}_j \underline{\otimes} \boldsymbol{G}_i). \end{aligned} \tag{1.10}$$

with $m_i = g + g_i$. The resulting coefficients are:

$$\lambda_{ii} = (\lambda_c + 2\mu_c) m_i^{2k}, \quad \lambda_{ij}^* = \lambda_c m_i^k m_j^k, \quad \mu_{ij} = \mu_c m_i^k m_j^k. \tag{1.11}$$

1.2.4 Positive Definiteness and Matrix Representation

The tensor $\mathbb{S}$ is positive definite if:

$$\boldsymbol{E} : \mathbb{S}\boldsymbol{E} > 0, \quad \forall \boldsymbol{E} \neq 0, \tag{1.12}$$

which leads to the following conditions in Voigt notation:

$$3\lambda_c + 2\mu_c > 0, \quad \mu_c > 0, \quad \forall k \neq 0. \tag{1.13}$$

Finally, under the assumption of orthotropic symmetry, the matrix representation of $\mathbb{S}$ is constructed by aligning the spectral basis of $\boldsymbol{G}$ with the coordinate axes.

The elastic coefficients are determined by the expressions above, and the resulting matrix can be used in practical numerical implementations.

1.2.5 Matrix Representation and Conditions

The matrix form of the elasticity tensor $\mathbb{S}$ is obtained in the principal frame of $\boldsymbol{G}$, where $\boldsymbol{G}_i = \boldsymbol{g}_i \otimes \boldsymbol{g}_i$ are aligned with the coordinate axes. When the basis aligns with the principal directions of $\boldsymbol{G}$, and under the homogeneity assumption $\mathbb{S}(\lambda g, \lambda \boldsymbol{G}) = \lambda^k \mathbb{S}(g, \boldsymbol{G})$, the 6×6 matrix form of $\boldsymbol{S}$ is given by:

$$\boldsymbol{S} = \begin{pmatrix} (\lambda_c + 2\mu_c)m_1^{2k} & \lambda_c m_1^k m_2^k & \lambda_c m_1^k m_3^k & 0 & 0 & 0 \\ \lambda_c m_2^k m_1^k & (\lambda_c + 2\mu_c)m_2^{2k} & \lambda_c m_2^k m_3^k & 0 & 0 & 0 \\ \lambda_c m_3^k m_1^k & \lambda_c m_3^k m_2^k & (\lambda_c + 2\mu_c)m_3^{2k} & 0 & 0 & 0 \\ 0 & 0 & 0 & 2\mu_c m_2^k m_3^k & 0 & 0 \\ 0 & 0 & 0 & 0 & 2\mu_c m_3^k m_1^k & 0 \\ 0 & 0 & 0 & 0 & 0 & 2\mu_c m_1^k m_2^k \end{pmatrix}$$

Chapter 2

Material Models and Strain Energy Densities

2.1 Foundations of Hyperelasticity and Material Characterization

In the realm of nonlinear elasticity, a special class of materials known as **Green elastic** or *hyperelastic* materials is identified by the existence of a scalar-valued function ϕ, the *strain energy density*, from which the stress response is derived. For such materials, the internal forces depend solely on the current configuration, described by the deformation gradient $\mathbf{F}$, and not on the path taken to reach it.

The strain energy function is typically expressed in terms of the principal invariants of the right Cauchy-Green deformation tensor $\mathbf{C} = \mathbf{F}^T\mathbf{F}$:

$$\phi = \phi(I_1, I_2, I_3)$$

Here, the invariants I_1, I_2, I_3 are given by:

$$I_1 = \text{tr}(\mathbf{C}) \tag{2.1}$$

$$I_2 = \frac{1}{2}\left[(\text{tr}(\mathbf{C}))^2 - \text{tr}(\mathbf{C}^2)\right] \tag{2.2}$$

$$I_3 = \det(\mathbf{C}) = J^2, \quad \text{with } J = \det(\mathbf{F}) \tag{2.3}$$

The Rivlin-Ericksen formulation for isotropic hyperelasticity allows the second Piola-Kirchhoff stress tensor $\mathbf{S}$ to be obtained directly from derivatives of ϕ with respect to these invariants:

$$\mathbf{S} = f\left(\frac{\partial\phi}{\partial I_1}, \frac{\partial\phi}{\partial I_2}, \frac{\partial\phi}{\partial I_3}\right)$$

Various models have been proposed to capture different hyperelastic responses through specific forms of ϕ. Some of the most commonly used are:

- **Neo-Hookean** model: captures moderate elasticity.
- **Mooney-Rivlin** model: offers better flexibility by incorporating more invariants.
- **Gent-Gent** model: accounts for limiting chain extensibility.
- **Ogden** model: suited for large nonlinear deformations via principal stretches.

These models are chosen based on the degree of nonlinearity and anisotropy observed in materials.

2.2 Strain Energy Potentials in Isotropic Hyperelasticity

The assumption of isotropy implies that the strain energy depends only on the scalar invariants of $\mathbf{C}$. Each model uses a distinct functional form of ϕ to characterize material behavior.

2.2.1 Neo-Hookean Model

One of the simplest models, the Neo-Hookean strain energy density function is:

$$\phi_{\mathrm{NH}} = c_1(I_1 - 3)$$

where c_1 is a material constant. It models rubber-like behavior under small to moderate strains but does not capture strain stiffening accurately.

2.2.2 Mooney-Rivlin Model

The Mooney-Rivlin model extends Neo-Hookean theory by including a dependence on I_2:

$$\phi_{\mathrm{MR}} = c_1(I_1 - 3) + c_2(I_2 - 3)$$

Here, c_1 and c_2 provide more flexibility to fit experimental data, especially in biaxial deformation scenarios.

2.2.3 Gent-Gent Model

To account for limiting extensibility in polymer chains, the Gent-Gent model modifies the energy function to become singular at a maximum extension limit:

$$\phi_{\mathrm{GG}} = -\frac{\mu J_m}{2} \ln\left(1 - \frac{I_1 - 3}{J_m}\right)$$

where μ is the shear modulus and J_m controls the maximum permissible value of I_1.

2.2.4 Ogden Model

Instead of invariants, the Ogden model uses the principal stretches $\lambda_1, \lambda_2, \lambda_3$ to express the energy:

$$\phi_{\mathrm{Ogden}} = \sum_{p=1}^{N} \frac{\mu_p}{\alpha_p} \left(\lambda_1^{\alpha_p} + \lambda_2^{\alpha_p} + \lambda_3^{\alpha_p} - 3\right)$$

Parameters μ_p and α_p are determined through fitting procedures and can effectively model highly nonlinear responses.

2.3 Anisotropy and Fabric Tensor Framework

While the aforementioned models assume isotropy, real materials, especially biological tissues and fibrous composites, exhibit direction-dependent responses. This anisotropy can be incorporated by introducing a *fabric tensor* $\mathbf{M}$, which encodes the preferred directions and structural information of the material.

A general representation of the fabric tensor is:

$$\mathbf{M} = g\mathbf{I} + \mathbf{G}$$

where g is an isotropic scalar, and $\mathbf{G}$ is a traceless symmetric tensor representing the deviation from isotropy.

In the reference configuration, $\mathbf{F} = \mathbf{I}$, so the right Cauchy-Green tensor becomes:

$$\mathbf{C} = \mathbf{I}, \quad \text{yielding } I_1 = 3, \quad I_2 = 3, \quad I_3 = 1$$

Substituting these into any of the strain energy functions yields zero, indicating the undeformed, stress-free state. Here $\mathbf{F}$ denotes the deformation gradient.

2.4 Stress Measures in the Reference Configuration

The *Green-Lagrange strain tensor* $\mathbf{E}$ provides a symmetric measure of strain relative to the reference configuration:

$$\mathbf{E} = \frac{1}{2}(\mathbf{C} - \mathbf{I})$$

Conjugate to $\mathbf{E}$ is the second Piola-Kirchhoff stress tensor $\mathbf{S}$, and the constitutive law for a hyperelastic solid can be written as:

$$\mathbf{S} = \mathbb{C} : \mathbf{E}$$

Here, $\mathbb{C}$ is the fourth-order elasticity tensor, which may vary with directionality in anisotropic materials.

2.5 Elasticity Tensor and Anisotropic Contributions

The elasticity tensor $\mathbb{C}$ reflects how microstructural features influence the global elastic behavior. By decomposing the fabric tensor $\mathbf{M}$ into its spectral components, with eigenvalues $m_i = g + g_i$ and corresponding projectors $\mathbf{G}_i = \mathbf{g}_i \otimes \mathbf{g}_i$, the tensor $\mathbb{C}$ can be expressed as:

$$\begin{aligned}\mathbb{C}(\mathbf{M}) = &\sum_i (\lambda_0 + 2\mu_0) m_i^{2k}\, \mathbf{G}_i \otimes \mathbf{G}_i \\ &+ \sum_{i<j} \lambda_0 m_i^k m_j^k (\mathbf{G}_i \otimes \mathbf{G}_j + \mathbf{G}_j \otimes \mathbf{G}_i) \\ &+ \sum_{i<j} \mu_0 m_i^k m_j^k \, (\mathbf{G}_i \otimes \mathbf{G}_j + \mathbf{G}_j \otimes \mathbf{G}_i)\end{aligned} \tag{2.4}$$

The last term involves the symmetric tensor product of $\mathbf{G}_i$ and $\mathbf{G}_j$, defined as:

$$\mathbf{A} \underset{-}{\otimes} \mathbf{B} = \frac{1}{2}(\mathbf{A} \otimes \mathbf{B} + \mathbf{B} \otimes \mathbf{A})$$

Such a formulation ensures that the stiffness contributions from various directional components are properly accounted for.

2.6 Coupling Microstructure with Stress Response

By integrating the fabric tensor into the constitutive model, the second Piola-Kirchhoff stress becomes sensitive to both strain and material anisotropy:

$$\mathbf{S} = \mathbb{C}(\mathbf{F}) : \mathbf{E}$$

This expression encapsulates the influence of directional microstructures, allowing for a more accurate prediction of stress under arbitrary deformations.

Assuming a reference density $\rho = 1$ simplifies the energy densities and stress expressions, focusing attention on the geometric and microstructural mechanisms driving the mechanical response.

Chapter 3

Strain Energy Density Manifold

3.1 Overview

In hyperelastic material modeling, the strain energy density function ϕ serves as a scalar potential that governs the stress-strain behavior of materials. It is typically expressed in terms of the invariants of the right Cauchy-Green deformation tensor $\mathbf{C} = \mathbf{F}^T\mathbf{F}$, where $\mathbf{F}$ is the deformation gradient. The three principal invariants of $\mathbf{C}$ are:

$$I_1 = \mathrm{tr}(\mathbf{C}) \tag{3.1}$$

$$I_2 = \frac{1}{2}\left[(\mathrm{tr}(\mathbf{C}))^2 - \mathrm{tr}(\mathbf{C}^2)\right] \tag{3.2}$$

$$I_3 = \det(\mathbf{C}) \tag{3.3}$$

The strain energy density is then defined as a function:

$$\phi = \phi(I_1, I_2, I_3) \tag{3.4}$$

However, it is important to note that the invariants I_1, I_2, I_3 are not entirely independent of each other. They are all derived from the same deformation tensor $\mathbf{C}$,

and thus are constrained by the underlying geometry and structure of the deformation space. As a result, the set of physically realizable invariant triplets (I_1, I_2, I_3) forms a submanifold of $\mathbb{R}^3$. The strain energy function is then effectively defined over this constrained subset of the full invariant space.

This perspective leads naturally to the idea of interpreting ϕ as a scalar field over this manifold of admissible invariants, rather than over the entire $\mathbb{R}^3$.

3.2 The Manifold Interpretation

3.2.1 Energy as a Field over Invariant Space

The strain energy function ϕ can be visualized as a scalar field defined over the space of invariants (I_1, I_2, I_3), subject to the constraint that these invariants are not independent. The set of all physically meaningful combinations of these invariants forms a smooth, constrained manifold in $\mathbb{R}^3$. Over this manifold, the function ϕ assigns a scalar energy value to each deformation state.

In many practical cases, such as modeling incompressible materials, this manifold becomes simpler. For incompressibility, the condition $\det(\mathbf{C}) = I_3 = 1$ must be satisfied, which reduces the dimensionality of the manifold to a two-dimensional surface embedded in $\mathbb{R}^3$.

3.2.2 Incompressibility and Dimensional Reduction

Assuming incompressibility, we fix $I_3 = 1$, simplifying the strain energy function to depend on only two variables:

$$\phi = \phi(I_1, I_2) \quad \text{with } I_3 = 1 \tag{3.5}$$

The resulting manifold $\mathcal{M}$ is a two-dimensional surface in (I_1, I_2, ϕ)-space. Each point on this surface corresponds to a unique deformation state consistent with the incompressibility constraint.

3.2.3 Visualization of the Energy Manifold

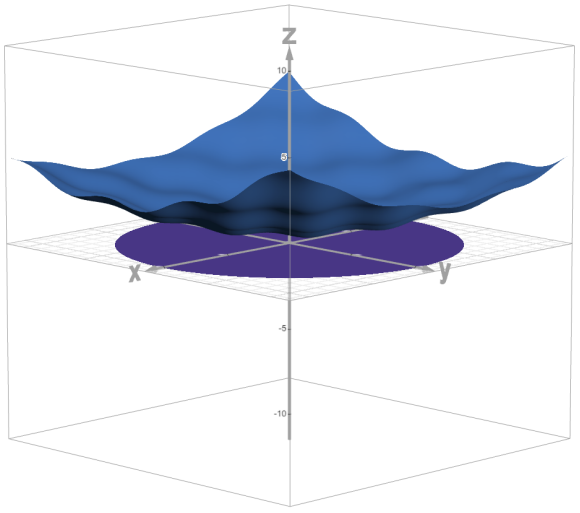

FIGURE 3.1: Close-up visualization of the strain energy density manifold $\mathcal{M}$. Each point on the surface represents a triplet (I_1, I_2, ϕ) under the constraint $I_3 = 1$.

Figure 3.1 presents a highly magnified view of the strain energy density manifold. Although the strain energy function $\phi(I_1, I_2)$ exhibits a complex and rapidly varying structure across the admissible domain, it continues to respect essential mathematical and physical properties:

- **Smoothness:** The function $\phi(I_1, I_2)$ remains differentiable throughout the domain, permitting consistent computation of stress and tangent moduli using first and second derivatives.
- **Continuity:** Despite its intricate behavior, the energy function does not exhibit discontinuities or singularities, ensuring physical realism and numerical stability.
- **Physical Validity:** The energy function correctly vanishes at the reference (undeformed) configuration:

$$\mathbf{F} = \mathbf{I} \Rightarrow \mathbf{C} = \mathbf{I} \Rightarrow I_1 = 3, \quad I_2 = 3, \quad I_3 = 1 \Rightarrow \phi = 0$$

3.3 Incomplete Knowledge of the Manifold in Real Materials

Although the manifold perspective provides a powerful geometric framework, the explicit form of the energy function $\phi(I_1, I_2)$ is generally unknown for real materials. Classical models such as Neo-Hookean and Mooney-Rivlin attempt to approximate this surface:

$$\phi_{\text{NH}} = c_1(I_1 - 3) \tag{3.6}$$

$$\phi_{\text{MR}} = c_1(I_1 - 3) + c_2(I_2 - 3) \tag{3.7}$$

While useful, these models often fail to fully capture the complexity of material behavior observed in experiments. Many materials exhibit non-trivial transitions across different deformation regimes, sensitivity to loading paths, strain rates, and evolving internal microstructure, all of which alter the true energy landscape.

Therefore, the actual energy manifold $\mathcal{M}$ is often only partially characterized by analytical models. Understanding and reconstructing the complete manifold requires data-driven methods capable of interpolating and generalizing from sparse or noisy experimental data.

3.4 Manifold Structure in Mooney-Rivlin Materials

To illustrate the concept of a strain energy manifold, consider the Mooney-Rivlin strain energy density function:

$$\phi_{\text{MR}} = c_1(I_1 - 3) + c_2(I_2 - 3) \tag{3.8}$$

where c_1 and c_2 are material constants, and the invariants I_1 and I_2 are defined from the right Cauchy-Green deformation tensor $\mathbf{C} = \mathbf{F}^T\mathbf{F}$. Under the assumption of incompressibility:

$$I_3 = \det(\mathbf{C}) = 1 \tag{3.9}$$

this constraint reflects the physical requirement that the material volume remains unchanged during deformation. That is, the deformation may alter the shape of a material element, but the volume must stay constant. Mathematically, this means that the product of the principal stretches $\lambda_1\lambda_2\lambda_3 = 1$, and hence the invariants I_1 and I_2, which are functions of these stretches, are not entirely independent. They are constrained to lie on a specific manifold in the (I_1, I_2) space, dictated by the incompressibility condition $\det(\mathbf{C}) = 1$.

3.4.1 Invariant Relations Under Incompressibility

To analyze the geometry of the strain energy manifold, we begin with the principal stretches $\lambda_1, \lambda_2, \lambda_3$, which are the square roots of the eigenvalues of the right Cauchy-Green deformation tensor $\mathbf{C} = \mathbf{F}^T\mathbf{F}$. Since $\mathbf{C}$ is symmetric and positive-definite, its eigenvalues are λ_i^2, and the principal invariants of $\mathbf{C}$ can be expressed in terms of the stretches as:

$$I_1 = \lambda_1^2 + \lambda_2^2 + \lambda_3^2 \tag{3.10}$$

$$I_2 = \lambda_1^2\lambda_2^2 + \lambda_2^2\lambda_3^2 + \lambda_3^2\lambda_1^2 \tag{3.11}$$

$$I_3 = \lambda_1^2\lambda_2^2\lambda_3^2 \tag{3.12}$$

Under the assumption of incompressibility, the material volume must remain unchanged during deformation. This implies that:

$$\det(\mathbf{F}) = \lambda_1\lambda_2\lambda_3 = 1 \tag{3.13}$$

Squaring both sides gives the incompressibility constraint in terms of $\mathbf{C}$:

$$I_3 = \det(\mathbf{C}) = 1 \tag{3.14}$$

This condition allows us to eliminate one of the stretches. Without loss of generality, we may write:

$$\lambda_3 = \frac{1}{\lambda_1 \lambda_2} \tag{3.15}$$

Substituting into the expressions for I_1 and I_2, we obtain:

$$I_1 = \lambda_1^2 + \lambda_2^2 + \left(\frac{1}{\lambda_1 \lambda_2}\right)^2 = \lambda_1^2 + \lambda_2^2 + \frac{1}{\lambda_1^2 \lambda_2^2} \tag{3.16}$$

$$I_2 = \lambda_1^2 \lambda_2^2 + \frac{1}{\lambda_1^2} + \frac{1}{\lambda_2^2} \tag{3.17}$$

Thus, under the incompressibility constraint, both I_1 and I_2 become functions of only two variables, λ_1 and λ_2, and the admissible set of (I_1, I_2) values forms a smooth two-dimensional surface in $\mathbb{R}^3$. This surface can be interpreted as the energy manifold over which the strain energy density $\phi(I_1, I_2)$ is defined.

3.4.2 Illustrative Case: Uniaxial Stretch

To further understand this geometry, consider the special case of a uniaxial stretch along the x-axis. Let λ denote the stretch in that direction. Incompressibility then enforces the lateral stretches as:

$$\lambda_1 = \lambda, \quad \lambda_2 = \lambda_3 = \lambda^{-1/2} \tag{3.18}$$

This corresponds to the following deformation gradient:

$$\mathbf{F} = \begin{pmatrix} \lambda & 0 & 0 \\ 0 & \lambda^{-1/2} & 0 \\ 0 & 0 & \lambda^{-1/2} \end{pmatrix} \tag{3.19}$$

Substituting into the invariants yields:

$$I_1 = \lambda^2 + 2\lambda^{-1} \tag{3.20}$$

$$I_2 = \lambda^{-2} + 2\lambda \tag{3.21}$$

This gives a parametric curve in the (I_1, I_2) plane, governed entirely by the scalar parameter λ. It further illustrates the constraint-driven relationship between I_1 and I_2, and reinforces the interpretation of the admissible domain as a manifold in invariant space.

3.4.3 Visualization of the Admissible Invariant Manifold

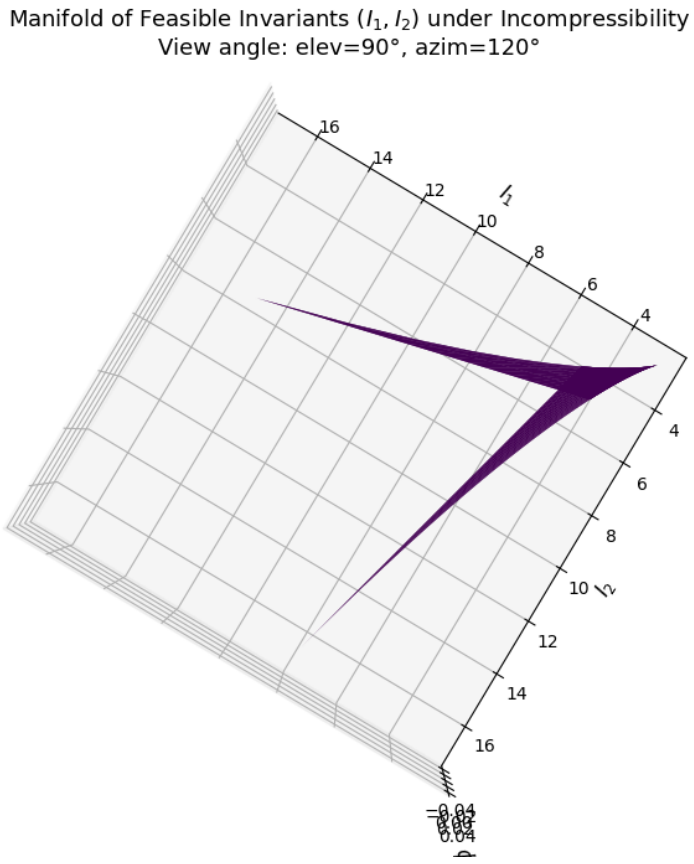

FIGURE 3.2: Surface of admissible invariant pairs (I_1, I_2) under the constraint $I_3 = 1$, constructed via principal stretches.

3.4.4 Strain Energy Density on the Manifold

Using the Mooney-Rivlin form of the strain energy density function, the energy is given by:

$$\phi(I_1, I_2) = c_1(I_1 - 3) + c_2(I_2 - 3) \tag{3.22}$$

To visualize this function over the admissible invariant manifold defined by $I_3 = 1$, we assign specific values to the material constants. For illustration purposes, we choose:

$$c_1 = 1, \quad c_2 = 0.5$$

With these values, the energy function becomes:

$$\phi(I_1, I_2) = (I_1 - 3) + 0.5(I_2 - 3) \tag{3.23}$$

This form is used to plot the energy landscape $\phi(I_1, I_2)$ over the two-dimensional surface of admissible (I_1, I_2) values, constrained by the incompressibility condition $I_3 = 1$.

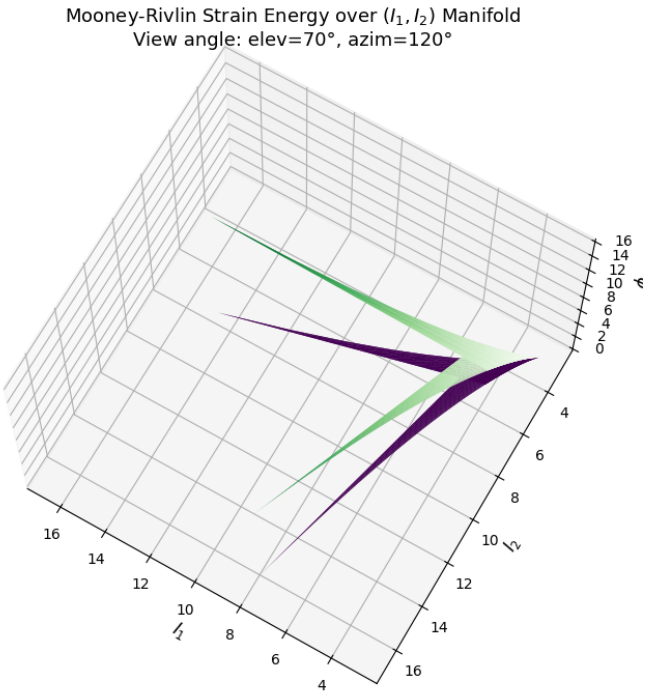

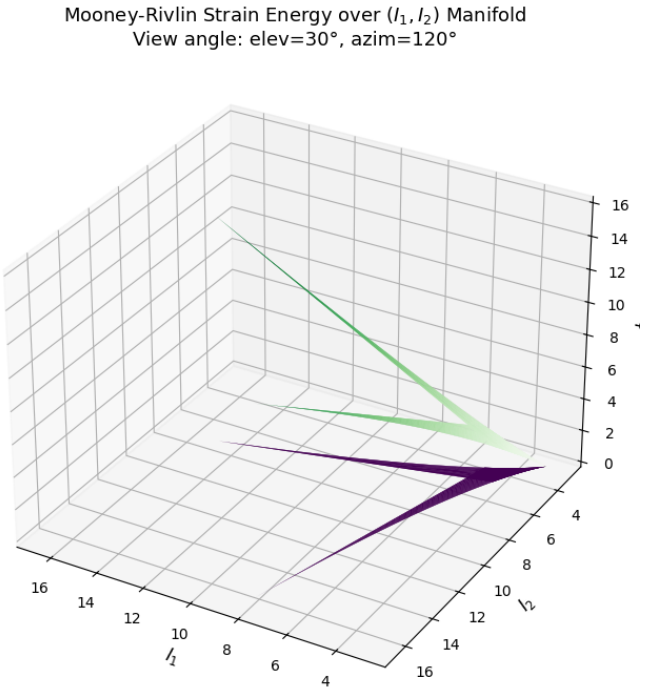

FIGURE 3.3: Strain energy density surface $\phi(I_1, I_2)$ for a Mooney-Rivlin material, plotted over the admissible invariant manifold from two different elevation angles to provide better geometric intuition.

Chapter 4

Computing the Fabric Tensor from Deformation Gradient

In this chapter, we describe how the fabric tensor $\mathbf{M}$ is computed from the deformation gradient tensor $\mathbf{F}$. While in theory $\mathbf{M}$ is often symmetric and idealized, numerical approximations involve working with general (possibly non-symmetric) deformation gradients. We explore both the classical polar decomposition method and a more efficient eigendecomposition-based technique.

4.1 Stress Computation from Numerical Deformation Gradient

Given a numerical value of the deformation gradient tensor $\mathbf{F}$, we compute the corresponding Mooney-Rivlin stress using a function:

4.1.1 Stress Computation from Numerical Deformation Gradient

Given a deformation gradient tensor $\mathbf{F}$, the right Cauchy-Green deformation tensor is defined as:

$$\mathbf{C} = \mathbf{F}^\top \mathbf{F}. \tag{4.1}$$

The Green-Lagrange strain tensor $\mathbf{E}$ is then given by:

$$\mathbf{E} = \frac{1}{2}(\mathbf{C} - \mathbf{I}). \tag{4.2}$$

The scalar invariants of $\mathbf{C}$ are defined as:

$$I_1 = \mathrm{tr}(\mathbf{C}), \tag{4.3}$$

$$I_2 = \frac{1}{2}\left(I_1^2 - \mathrm{tr}(\mathbf{C}^2)\right), \tag{4.4}$$

$$I_3 = \det(\mathbf{C}). \tag{4.5}$$

The strain energy density function ϕ for a compressible Mooney-Rivlin material is expressed in terms of these invariants as:

$$\phi(I_1, I_2, I_3) = c_{10}\left(I_1 I_3^{-1/3} - 3\right) + c_{01}\left(I_2 I_3^{-2/3} - 3\right) + \frac{1}{D_1}\left(I_3^{1/2} - 1\right)^2, \tag{4.6}$$

where c_{10}, c_{01}, D_1 are material constants.

The derivatives of ϕ with respect to the invariants are then:

$$\frac{\partial \phi}{\partial I_1} = c_{10} \cdot I_3^{-1/3}, \tag{4.7}$$

$$\frac{\partial \phi}{\partial I_2} = c_{01} \cdot I_3^{-2/3}, \tag{4.8}$$

$$\frac{\partial \phi}{\partial I_3} = -\frac{1}{3} c_{10} I_1 I_3^{-4/3} - \frac{2}{3} c_{01} I_2 I_3^{-5/3} + \frac{1}{D_1}\left(1 - I_3^{-1/2}\right). \tag{4.9}$$

Using these expressions, the second Piola-Kirchhoff stress tensor $\mathbf{S}$ is computed as:

$$\mathbf{S} = 2\left[\left(\frac{\partial\phi}{\partial I_1} + I_1\frac{\partial\phi}{\partial I_2}\right)\mathbf{I} - \frac{\partial\phi}{\partial I_2}\mathbf{C} + \frac{\partial\phi}{\partial I_3}I_3\,\mathbf{C}^{-1}\right]. \tag{4.10}$$

This formulation allows evaluation of stress under large deformations, as governed by the Mooney-Rivlin model.

For numerical simulations, the material constants used are:

$$c_{10} = 32, \quad c_{01} = 8, \quad D_1 = \frac{1}{100}.$$

Before computing $\mathbf{S}$, it is also necessary to determine the fabric tensor $\mathbf{M}$, which depends on the left stretch tensor $\mathbf{V}$. The tensor $\mathbf{V}$ is obtained from the polar decomposition of the deformation gradient:

$$\mathbf{F} = \mathbf{VR}, \tag{4.11}$$

where $\mathbf{R}$ is a proper orthogonal rotation tensor.

4.2 Polar Decomposition and the Left Stretch Tensor

Let $\mathbf{F}$ be the deformation gradient. Then by polar decomposition, we have:

$$\mathbf{F} = \mathbf{RU} = \mathbf{VR} \tag{4.12}$$

where:

- $\mathbf{R}$: a proper orthogonal rotation tensor ($\mathbf{RR}^T = \mathbf{I}$, $\det\mathbf{R} = 1$)
- $\mathbf{U}$: right stretch tensor (symmetric and positive-definite)
- $\mathbf{V}$: left stretch tensor (symmetric and positive-definite)

Now, define the left Cauchy-Green deformation tensor:

$$\mathbf{B} = \mathbf{F}\mathbf{F}^T = \mathbf{V}^2 \tag{4.13}$$

Thus, the left stretch tensor is given by the matrix square root:

$$\mathbf{V} = \sqrt{\mathbf{B}} \tag{4.14}$$

4.2.1 Computing the Matrix Square Root $\sqrt{\mathbf{B}}$

For a symmetric, positive-definite tensor $\mathbf{B}$, the square root $\mathbf{V}$ is uniquely defined and can be computed by:

1. Diagonalizing $\mathbf{B}$: $\mathbf{B} = \mathbf{Q}\mathbf{\Lambda}\mathbf{Q}^T$, where $\mathbf{\Lambda} = \text{diag}(\lambda_1^2, \lambda_2^2, \lambda_3^2)$
2. Taking the square root of the eigenvalues: $\sqrt{\mathbf{\Lambda}} = \text{diag}(\lambda_1, \lambda_2, \lambda_3)$
3. Reconstructing $\mathbf{V}$:
$$\mathbf{V} = \mathbf{Q}\sqrt{\mathbf{\Lambda}}\mathbf{Q}^T \tag{4.15}$$

4.3 Fabric Tensor from the Stretch Tensor

Once $\mathbf{V}$ is computed, the fabric tensor $\mathbf{M}$ is defined as:

$$\mathbf{M} = \frac{3}{\text{tr}(\mathbf{V})}\mathbf{V} \tag{4.16}$$

This normalizes $\mathbf{V}$ such that $\text{tr}(\mathbf{M}) = 3$, ensuring isotropic weighting in the undeformed state where $\mathbf{F} = \mathbf{I} \Rightarrow \mathbf{V} = \mathbf{I}$.

4.4 Eigenvalue-Based Simplification of the Fabric Tensor

A more computationally efficient method uses the eigendecomposition of $\mathbf{B}$. Let the eigenvalues of $\mathbf{B}$ be $\lambda_1^2, \lambda_2^2, \lambda_3^2$, and corresponding orthonormal eigenvectors be $\mathbf{e}_1, \mathbf{e}_2, \mathbf{e}_3$. Then:

$$\mathbf{B} = \sum_{i=1}^{3} \lambda_i^2 \, \mathbf{e}_i \otimes \mathbf{e}_i \tag{4.17}$$

$$\mathbf{V} = \sum_{i=1}^{3} \lambda_i \, \mathbf{e}_i \otimes \mathbf{e}_i \tag{4.18}$$

Then the fabric tensor becomes:

$$\mathbf{M} = \frac{3}{\lambda_1 + \lambda_2 + \lambda_3} \sum_{i=1}^{3} \lambda_i \, \mathbf{e}_i \otimes \mathbf{e}_i \tag{4.19}$$

This approach avoids computing full matrix square roots and only requires spectral decomposition of the symmetric matrix $\mathbf{B}$, which is numerically stable and efficient.

Chapter 5

Residual Energy Function and Elasticity Tensor Construction

In previous chapters, we discussed the derivation of the second Piola-Kirchhoff stress tensor $\mathbf{S}$ from a strain energy density function and introduced the elasticity tensor $\mathbb{C}$, which links the Green-Lagrange strain tensor $\mathbf{E}$ to the stress via constitutive relations.

This chapter introduces the *residual energy function*, a scalar-valued function that quantifies the deviation between observed stress and stress predicted by a constitutive model. It serves as a loss function in material parameter calibration and model validation.

5.1 Residual Energy Density

5.1.1 General Definition

The residual energy density ψ is defined as:

$$\psi = W + W^* - \boldsymbol{\sigma} : \boldsymbol{\varepsilon}$$

where:

- $W = \int_0^{\boldsymbol{\varepsilon}} \boldsymbol{\sigma} : d\boldsymbol{\varepsilon}$ is the strain energy,
- $W^* = \int_0^{\boldsymbol{\sigma}} \boldsymbol{\varepsilon} : d\boldsymbol{\sigma}$ is the complementary energy,
- $\boldsymbol{\sigma} : \boldsymbol{\varepsilon}$ is the total work done.

5.1.2 Linear Elastic Case

For a linear elastic material:

$$\boldsymbol{\sigma} = \mathbb{C} : \boldsymbol{\varepsilon}, \quad \boldsymbol{\varepsilon} = \mathbb{C}^{-1} : \boldsymbol{\sigma}$$

$$W = \frac{1}{2}\boldsymbol{\varepsilon} : \mathbb{C} : \boldsymbol{\varepsilon}, \quad W^* = \frac{1}{2}\boldsymbol{\sigma} : \mathbb{C}^{-1} : \boldsymbol{\sigma}$$

$$\Rightarrow \psi = \frac{1}{2}\boldsymbol{\varepsilon} : \mathbb{C} : \boldsymbol{\varepsilon} + \frac{1}{2}\boldsymbol{\sigma} : \mathbb{C}^{-1} : \boldsymbol{\sigma} - \boldsymbol{\sigma} : \boldsymbol{\varepsilon}$$

5.1.3 General Form (Nonlinear Case)

Rewriting the residual in compact quadratic form:

$$\psi = \frac{1}{2}\left(\boldsymbol{\sigma} - \mathbb{C} : \boldsymbol{\varepsilon}\right) : \mathbb{C}^{-1} : \left(\boldsymbol{\sigma} - \mathbb{C} : \boldsymbol{\varepsilon}\right)$$

5.1.4 Physical Interpretation

- $\psi = 0$ for perfect linear elasticity.
- $\psi > 0$ indicates deviation from the model.
- Being a quadratic form, ψ is always non-negative.

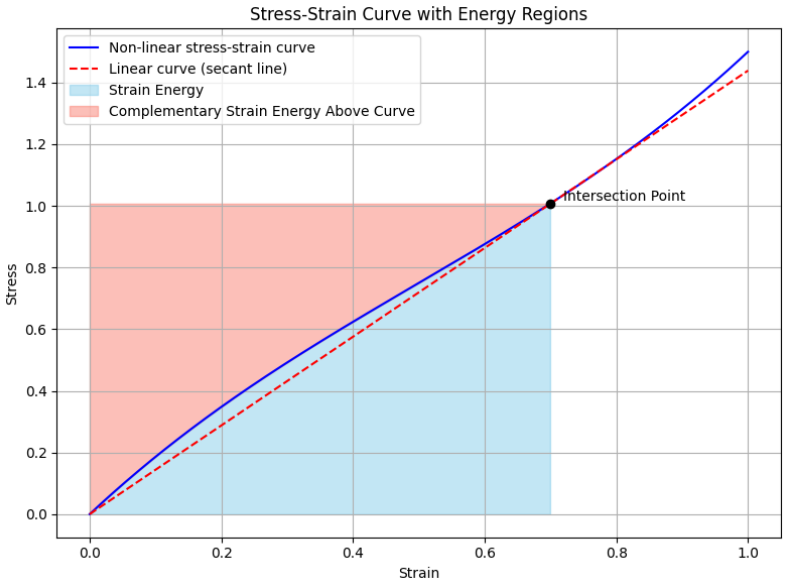

FIGURE 5.1: Residual energy construction from strain and complementary energy.

5.1.5 Graphical Interpretation

5.2 Residual Function Using Second Piola-Kirchhoff Stress

$$\psi = \frac{1}{2}\left(\mathbf{S} - \mathbb{C} : \mathbf{E}\right) : \mathbb{C}^{-1} : \left(\mathbf{S} - \mathbb{C} : \mathbf{E}\right)$$

Here:

- $\mathbf{S}$: Second Piola-Kirchhoff stress tensor,
- $\mathbf{E}$: Green-Lagrange strain tensor,
- $\mathbb{C}$: Fourth-order elasticity tensor.

Minimizing ψ aligns model predictions with observed stress.

5.3 Elasticity Tensor Construction via Fabric Tensor

5.3.1 Fabric Tensor Definition

Let $\mathbf{M}$ be a symmetric second-order fabric tensor with spectral decomposition:

$$\mathbf{M} = \sum_{i=1}^{3} \lambda_i \, \mathbf{e}_i \otimes \mathbf{e}_i$$

5.3.2 Tensorial Basis

- Second-order: $\mathbf{M}_i = \mathbf{e}_i \otimes \mathbf{e}_i$
- Fourth-order:

$$\mathbb{M}_{ii} = \mathbf{M}_i \otimes \mathbf{M}_i, \quad \mathbb{M}_{ij} = \mathbf{M}_i \otimes \mathbf{M}_j, \quad \mathbb{M}^s_{ij} = \mathbf{M}_i \underline{\bar{\otimes}} \mathbf{M}_j$$

5.3.3 Elasticity Tensor Components

Directional Contribution:

$$\mathbb{C}^{(1)} = (\lambda_0 + 2\mu_0) \sum_{i=1}^{3} \lambda_i^{2\exp} \mathbb{M}_{ii}$$

Cross-Coupling:

$$\mathbb{C}^{(2)} = \lambda_0' \sum_{i \neq j} (\mathbb{M}_{ij} + \mathbb{M}_{ji})$$

Mixed Symmetric Contribution:

$$\mathbb{C}^{(3)} = 2\mu_0 \sum_{i \neq j} (\lambda_i \lambda_j)^{\alpha} \left(\mathbb{M}^s_{ij} + \mathbb{M}^s_{ji} \right)$$

5.3.4 Final Expression

$$\mathbb{C} = \mathbb{C}^{(1)} + \mathbb{C}^{(2)} + \mathbb{C}^{(3)}$$

5.4 Numerical Representation via Voigt Notation

To facilitate computation, tensors are mapped to matrix form using Voigt notation.

- Symmetric 2nd-order tensors $\rightarrow$ 6D vectors
- 4th-order tensors $\rightarrow 6 \times 6$ matrices

Mapping:

$$\begin{array}{ccc} (0,0) \rightarrow 0, & (1,1) \rightarrow 1, & (2,2) \rightarrow 2, \\ (1,2), (2,1) \rightarrow 3, & (0,2), (2,0) \rightarrow 4, & (0,1), (1,0) \rightarrow 5 \end{array}$$

Residual energy becomes:

$$\psi = \frac{1}{2}(\vec{S} - \mathbf{C}\vec{E})^\top \mathbf{C}^{-1} (\vec{S} - \mathbf{C}\vec{E})$$

5.5 Minimization Objective

The objective function ψ is minimized individually at each of the 14,696 Gauss points, which are discrete integration points within the finite element mesh. For each Gauss point, the following minimization problem is solved:

$$\min_{\theta} \psi^{(i)}(\theta),$$

where $\theta = (\lambda_0, \mu_0, \lambda_0', k)$ represents the material parameters corresponding to the i^{th} Gauss point. This minimization is performed across all 10 loading steps, ensuring that the optimized parameters $\mathbb{C}(\theta)$ accurately reflect the observed stress-strain behavior throughout the loading history.

5.6 Visualization of Gauss Points in the Plate with a Hole

To contextualize the parameter optimization process, the following figures show the distribution of all 14,696 Gauss points in the finite element mesh of the plate-with-a-hole geometry. Each Gauss point corresponds to an integration point where stress and strain are evaluated and optimized.

The structure is stretched in the Y-direction with a stretch ratio of 2, resulting in a vertically elongated configuration. Visualizing these points helps to understand the spatial resolution and coverage of the optimization.

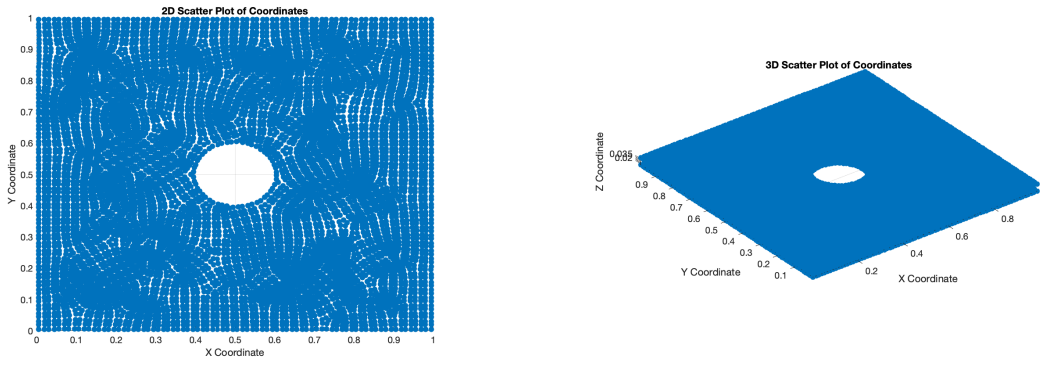

(a) 2D view of Gauss points

(b) 3D view of Gauss points

FIGURE 5.2: Distribution of Gauss points in the plate-with-a-hole geometry stretched in the Y-direction by a factor of 2.

Chapter 6

Optimization of Material Parameters

The mechanical response of anisotropic materials is governed by their internal microstructure. To model this behavior accurately, a set of material parameters defining the constitutive law must be calibrated. This chapter presents the formulation and implementation of an optimization framework for estimating these parameters using experimental or simulated stress-strain data.

6.1 Problem Formulation

6.1.1 Material Parameters

The following four parameters characterize the anisotropic elastic behavior:

$$\lambda_o, \quad \mu_o, \quad \lambda_o^\star, \quad k$$

These appear in the formulation of the fourth-order stiffness tensor $\mathbb{C}$. It governs the linear stress-strain relationship.

6.1.2 Residual Energy Functional

To quantify the mismatch between observed and predicted strains under a given stress, we define the residual energy functional:

$$\psi(\lambda_o, \mu_o, \lambda_o^\star, k) = \frac{1}{2}(\vec{S} - \mathbf{C}\vec{E})^\top \mathbf{C}^{-1} (\vec{S} - \mathbf{C}\vec{E}),$$

where:

- $\vec{E}$, $\vec{S}$: strain and stress vectors in Voigt notation,
- $\mathbf{C}$: 6×6 stiffness matrix derived from $\mathbb{C}$.

This functional penalizes the error between predicted and observed strain, scaled appropriately by the material stiffness.

6.2 Optimization Strategy

6.2.1 Optimization Method

We employ constrained optimization using MATLAB's `fmincon` solver to minimize the residual energy functional

$$\psi(\lambda_o, \mu_o, \lambda_o^\star, k) = \frac{1}{2} \left\| \vec{S} - \mathbf{C}(\lambda_o, \mu_o, \lambda_o^\star, k)\vec{E} \right\|^2,$$

where $\vec{E}$ and $\vec{S}$ are the strain and stress vectors in Voigt notation, respectively, and $\mathbf{C}$ is the stiffness matrix constructed from the parameters and the eigenstructure of the fabric tensor.

The optimization incorporates nonlinear inequality constraints to ensure physical admissibility of the material parameters. Specifically, the following constraints are enforced:

$$3\lambda_o + 2\mu_o > 0, \quad \mu_o > 0, \quad k > 0, \tag{6.1}$$

where λ_o and μ_o are the Lamé parameters and k is an additional model parameter.

The first inequality ensures that the *bulk modulus* $K = \lambda_o + \frac{2}{3}\mu_o$ is positive, which guarantees the material's resistance to volumetric compression and thus physical stability. The second condition, $\mu_o > 0$, enforces a positive shear modulus, ensuring the material resists shear deformations. Lastly, $k > 0$ ensures the physical relevance and stability of the model, associated with material nonlinearity.

The objective function is evaluated using a custom routine `objective_function`, and optimization is initialized with the guess:

$$\lambda_o^{(0)} = 1.0, \quad \mu_o^{(0)} = 1.0, \quad \lambda_o^{\star(0)} = 0.8, \quad k^{(0)} = 2.0.$$

Optimization options are configured with high-precision tolerances: `TolFun` and `TolX` set to 10^{-12}, and the display output is turned off.

6.2.2 Implementation Details

The optimization is conducted for each sample independently. The stress and strain components, along with the eigenstructure of the fabric tensor, are read from a CSV file. The results, including optimized parameters and energy values, are stored and merged back into the original dataset.

The constraints are implemented in matrix form as:

$$A = \begin{bmatrix} -3 & -2 & 0 & 0 \\ 0 & -1 & 0 & 0 \\ 0 & 0 & 0 & -1 \end{bmatrix}, \quad \vec{b} = \begin{bmatrix} -\epsilon \\ -\epsilon \\ -\epsilon \end{bmatrix}, \quad \epsilon = 10^{-12},$$

such that $A\vec{x} \leq \vec{b}$ ensures all inequality constraints are satisfied strictly.

The optimization proceeds as follows:

Algorithm 1 Parameter Optimization via Constrained Minimization

Input: CSV file with stress-strain data and fabric tensor eigenstructure
Output: Optimized parameters $\lambda_o, \mu_o, \lambda_o^\star, k$ for each data point
for $i = 1$ to N **do**
    Extract $\vec{E}_i$, $\vec{S}_i$, and fabric eigenstructure from row i
    Set initial guess $x_0 = [1.0, 1.0, 0.8, 2.0]$
    Define bounds: $[-\infty, 0, -\infty, 0] \leq \vec{x} \leq [\infty, \infty, \infty, \infty]$
    Define constraint matrix A and vector $\vec{b}$
    Minimize ψ using `fmincon(fun, x0, A, b, [], [], lb, ub, [], options)`
    if converged **then**
        Store optimized parameters and energy value
    else
        Log failure type according to exit flag
    end if
end for
Merge results with original dataset and export to CSV

This algorithm offers a systematic approach to calibrate anisotropic elasticity parameters by minimizing a physically informed objective function under inequality constraints. The method processes each data point independently, enforcing bounds and constraints to guarantee physically admissible parameters. Failures during optimization are logged for further analysis, enhancing robustness. By integrating the optimized parameters with the original dataset, the approach yields physically interpretable results that can be readily applied in constitutive modeling, ensuring stability and consistency with observed stress-strain responses.

Chapter 7

Results and Discussion

7.1 Results and Discussion

7.1.1 Visualization of Von Mises Stress for 10 Loading Steps

To assess the accuracy of the optimized parameters, a standard plate-with-a-hole problem is simulated under 10 incremental loading steps. For each step, the stress distribution is evaluated using both the high-fidelity model and the approximated model obtained from the optimized parameters.

Instead of displaying all six individual stress components, the scalar field of von Mises stress is visualized. This quantity serves as a widely used criterion for yielding in ductile materials. The von Mises stress σ_{vm} is computed as:

$$\sigma_{vm} = \sqrt{\frac{1}{2}\left[(\sigma_{11} - \sigma_{22})^2 + (\sigma_{22} - \sigma_{33})^2 + (\sigma_{33} - \sigma_{11})^2\right] + 3(\sigma_{12}^2 + \sigma_{13}^2 + \sigma_{23}^2)}.$$

For each loading step, three contour plots are presented, based on values evaluated at Gauss points:

- **Original von Mises stress**
- **Approximated von Mises stress**

- **Error between original and approximated stress**

The resulting visualizations illustrate the comparison for all 10 loading steps. The color scale in each plot reflects the intensity of stress at individual Gauss points.

Contour Plot Comparisons for 10 Loading Steps (Plate with Hole)

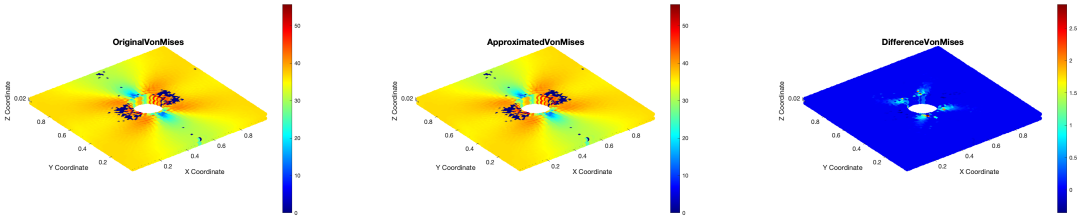

(a) Original von Mises Stress (b) Approximated von Mises Stress (c) Error in Approximation

FIGURE 7.1: Loading Step 1

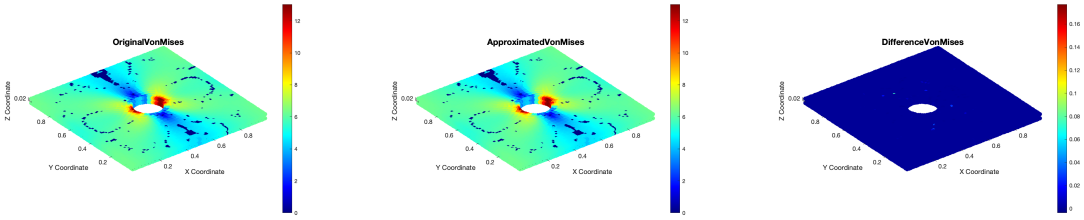

(a) Original von Mises Stress (b) Approximated von Mises Stress (c) Error in Approximation

FIGURE 7.2: Loading Step 2

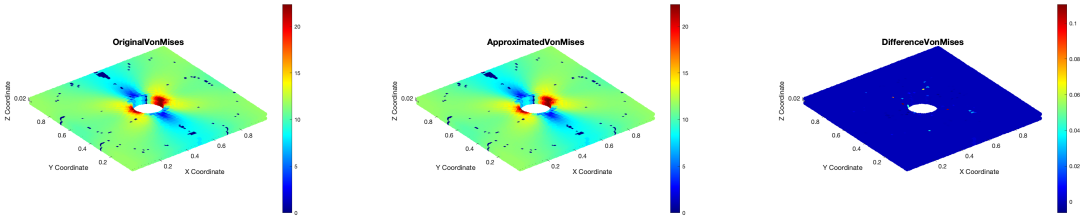

(a) Original von Mises Stress (b) Approximated von Mises Stress (c) Error in Approximation

FIGURE 7.3: Loading Step 3

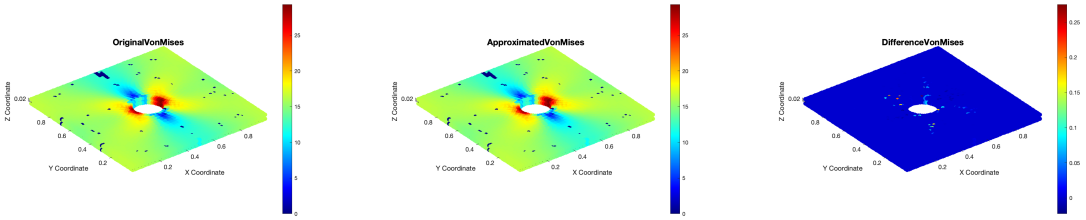

(a) Original von Mises Stress (b) Approximated von Mises Stress (c) Error in Approximation

FIGURE 7.4: Loading Step 4

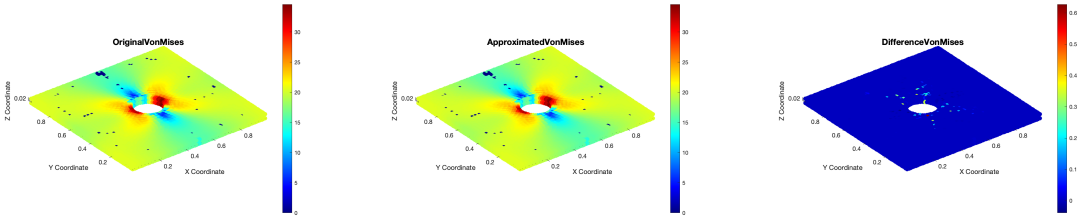

(a) Original von Mises Stress (b) Approximated von Mises Stress (c) Error in Approximation

FIGURE 7.5: Loading Step 5

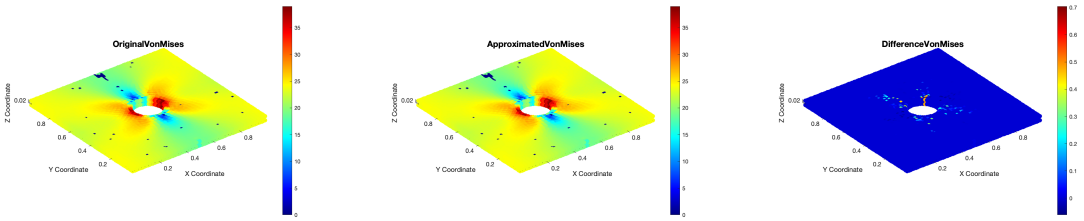

(a) Original von Mises Stress (b) Approximated von Mises Stress (c) Error in Approximation

FIGURE 7.6: Loading Step 6

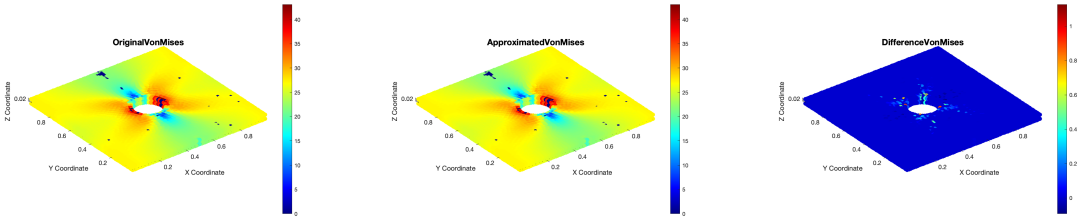

(a) Original von Mises Stress (b) Approximated von Mises Stress (c) Error in Approximation

FIGURE 7.7: Loading Step 7

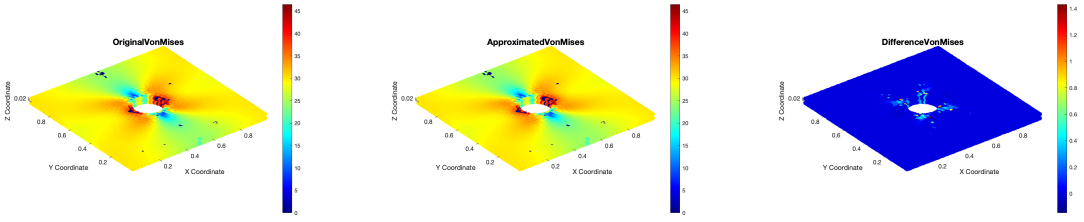

(a) Original von Mises Stress (b) Approximated von Mises Stress (c) Error in Approximation

FIGURE 7.8: Loading Step 8

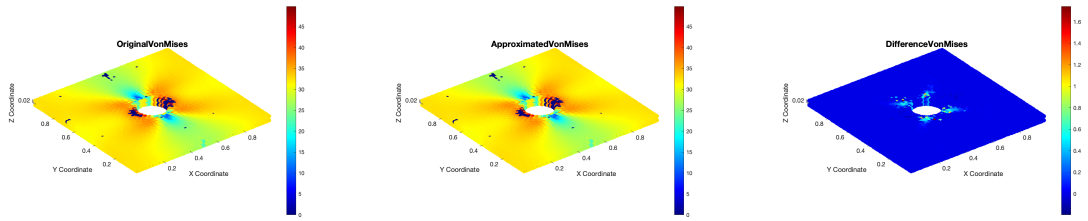

(a) Original von Mises Stress (b) Approximated von Mises Stress (c) Error in Approximation

FIGURE 7.9: Loading Step 9

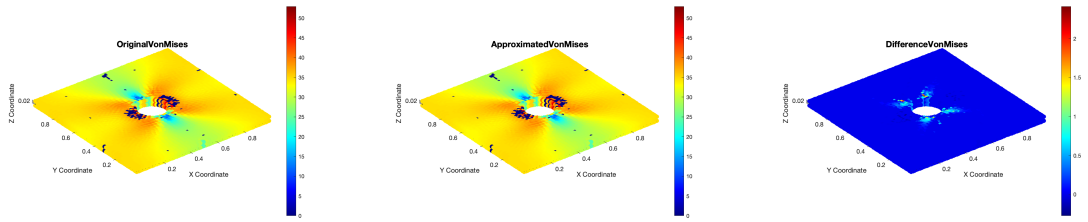

(a) Original von Mises Stress (b) Approximated von Mises Stress (c) Error in Approximation

FIGURE 7.10: Loading Step 10

Stress evaluation at Gauss points, which are the integration points within finite elements, provides more accurate results compared to nodal values. This is because Gauss points are specifically chosen for numerical integration, capturing the stress state more precisely inside the element and avoiding interpolation errors or smoothing effects that occur at the nodes. Consequently, stress contours plotted at Gauss points offer a more reliable representation of the material response.

7.1.2 Remarks and Future Work

The current approximation shows a reasonable match with the original stress response, especially in the bulk of the domain. However, boundary regions may show slight deviations due to limitations in convergence and numerical tolerances.

A few observations and suggestions for future improvement:

- **Increase Function Evaluations:** Some optimization iterations terminate prematurely. Raising the allowed function evaluations and iterations could improve convergence.
- **Optimization Strategy:** Switching to global optimizers like `ga` (genetic algorithm) or hybrid strategies may avoid local minima traps and improve reliability.
- **Neighborhood Averaging:** Since material properties do not vary drastically over small neighborhoods, averaging stress across neighboring Gauss points may yield smoother and more reliable approximations.

7.1.3 Comparison with Machine Learning Approaches

While machine learning models (e.g., neural networks) have been proposed for stress prediction at Gauss points, they suffer from interpretability issues and often require hundreds of parameters for each point.

- **Physics-Informed:** Our model is grounded in physical constraints and constitutive theory, not data fitting alone.
- **Low Parameter Count:** Only 4 interpretable parameters ($\lambda_o, \mu_o, \lambda_o^\star, k$) are required, in contrast to black-box models.
- **Computationally Efficient:** Our optimization-based method is lightweight and can be integrated into simulations with minimal overhead.
- **Interpretability:** Each parameter has a clear mechanical meaning, aiding material design and diagnosis.

7.1.4 Conclusion

The presented method serves as a physically constrained, interpretable, and efficient alternative to data-driven machine learning models for stress approximation in anisotropic materials. Future work will include comparative studies with state-of-the-art ML models to benchmark accuracy, robustness, and computational cost.

Bibliography

Benoît, C. (1924). Sur la résolution numérique des systèmes d'équations linéaires. *Bulletin géodésique*, 2:67–77.

Boehler, J. P. (1987). Representation of constitutive laws. *Applied Mechanics Reviews*, 40(5):1059–1070.

Cowin, S. C. (1985a). The relationship between the elasticity tensor and the fabric tensor. *Mechanics of Materials*, 4(2):137–147.

Cowin, S. C. (1985b). The relationship between the elasticity tensor and the fabric tensor. *Mechanics of Materials*, 4(2):137–147.

Demmel, J. W. (1997). *Applied Numerical Linear Algebra*. Society for Industrial and Applied Mathematics.

Golub, G. H. and Van Loan, C. F. (1996). *Matrix Computations*. Johns Hopkins University Press, 3rd edition.

Higham, N. J. (2002). *Accuracy and Stability of Numerical Algorithms*. Society for Industrial and Applied Mathematics, 2nd edition.

Horn, R. A. and Johnson, C. R. (1985). *Matrix Analysis*. Cambridge University Press.

Kanatani, K. (1984). *Stereological methods applied to anisotropic structures*. MIT Press.

Mehrabadi, M. M. and Cowin, S. C. (1987). Eigentensors of linear anisotropic elastic materials. *Quarterly of Applied Mathematics*, 45(4):793–800.

Meyer, C. D. (2000). *Matrix Analysis and Applied Linear Algebra*. Society for Industrial and Applied Mathematics.

Parlett, B. N. (1998). *The Symmetric Eigenvalue Problem*. Society for Industrial and Applied Mathematics.

Stewart, G. W. (1998). *Matrix Algorithms: Volume I: Basic Decompositions*. Society for Industrial and Applied Mathematics.

Sylvester, J. J. (1852). A demonstration of the theorem that every homogeneous quadratic polynomial is reducible by real orthogonal substitutions to the form of a sum of positive and negative squares. *Philosophical Magazine Series 4*, 4(23):138–142.

Trefethen, L. N. and Bau, D. (1997). *Numerical Linear Algebra*. Society for Industrial and Applied Mathematics.

Varga, R. S. (1962). *Matrix Iterative Analysis*. Prentice-Hall.

Zysset, P. K. and Curnier, A. (1995). An alternative model for anisotropic elasticity based on fabric tensors. *Mechanics of Materials*, 21(3):243–250.